Original Article: High-yield Production of Amorphous Carbon via Ball Milling of Graphite and Prediction of Its Crystallite Size through ANN

Seyed Oveis Mirabootalebi*, |Gholam Hosien Akbari Fakhrabadi | Reza Mirahmadi Babaheydari

Department of materials & Metallurgy, Shahid Bahonar University of Kerman, Kerman, Iran

Use yor device to scan and read the article online

Citation S.O. Mirabootalebi*, G.H. Akbari, R.M. Babaheydari, **High-yield Production of Amorphous Carbon via Ball Milling of Graphite and Prediction of Its Crystallite Size through ANN**. *J. Appl. Organomet. Chem.*, **2021**, *1*(2), 76-85.

http://dx.doi.org/10.22034/jaoc.2021.288020.1021

Article info:
Received: 15 February 2021
Accepted: 21 March 2021
Available Online: 26 May 2021
ID: JAOC-2105-1021
Checked for Plagiarism: Yes
Peer Reviewers Approved by:
Dr. SUNIL V. GAIKWAD
Editor who Approved Publication:
Prof. Dr. Abdelkader Zarrouk

Keywords:
Amorphous carbon; Nanostructured carbon; Milling of graphite; Prediction crystallite size of carbon

ABSTRACT

One of the main methods for the synthesis of amorphous and nanostructured carbon is the mechanical milling of graphite. However, calculation and anticipation of the amorphous phase during the mechanical milling of graphite still is a major challenge due to a lot of important parameters. The main aim of this study is to mass-produce amorphous carbon and predict the crystallite size of graphite. For this purpose, ball-milling of graphite powder was carried out at different times of milling. The destruction of crystal structure and changes in phases were evaluated using X-ray diffraction (XRD), transmission electron microscope (TEM), atomic force microscopy (AFM), scanning electron microscope (SEM), and Zeta Seizer analysis. The results of the Material Analysis Using Diffraction (MAUD) for the obtained XRD patterns revealed that 91% and 93% of the unmilled graphite were converted to amorphous carbon at 250 and 330 h of ball-milling, respectively. To predict the crystallite size of carbon during the high energy ball-milling, the effective variables in the ball-milling process along with the initial crystallite size of carbon were determined as the input of the artificial neural network (ANN). Moreover, the final crystallite size of carbon was considered as the output of the network. The designed network with a root mean square error (RMSE) of 4% was able to predict the crystallite size of carbon during the process. Finally, by comparing the experimental results and the designed model, it was demonstrated that the predicted results were very close to the experimental outcomes. Accordingly, the presented model can be used for predicting the crystallite size of carbon during the mechanical milling of graphite.

Introduction

Amorphous carbon (AC) and nanostructured carbon owing to sp2 hybrid orbital components, high surface area. disorder and activated structure; have various properties such as high abrasion resistance, high porosity, and other mechanical, thermal and optical properties [1,2]. Likewise, some of the most important applications of amorphous and nanostructured carbon including use in solar cells [3], hydrogen

***Corresponding Author:** Seyed Oveis Mirabootalebi (oveis@eng.uk.ac.ir)*

storage materials [4], field-emitting displays [5], fabrication of carbon nanotubes [6], and buckypaper [7]. Various methods have been utilized to modify the crystalline structure of carbon; however, converting crystalline to the amorphous and nanostructured forms of carbon is one of the most common ways to produce AC. These techniques include CVD and laser-assisted CVD [8,9], laser ablation [10], arc discharge [11], flame [12], electrolysis [13], and milling of graphite [14]. Nevertheless, some key factors in mechanical activation (MA) such as the high potential for mass production, economic and simple process, make graphite milling one of the main approaches for the synthesis of amorphous and nanostructured carbon [15, 16].

Ball-milling of graphite always accompanies by a continuous decrease in the crystallite size of carbon. Therefore, the ordered structure of graphite converts to the nanostructured and amorphous phase by increasing the milling time. Determining the exact amount of nanostructure and amorphous phase and also predicting the crystallite size of carbon during ball-milling can lead to optimal usage of the process for a wide range of applications. Despite extensive research on the synthesis and characterization of amorphous carbon in the MA [15,17-19], no study was performed to specify the percentage of the produced nanostructured and amorphous phases. In addition, there are a lot of major factors in the ball-milling procedure. Hence, predicting the properties of the product such as the crystal size and the amount of amorphous phase is very difficult.

Numerous machine-learning models have been developed for optimization of the process and prediction of the major variables in materials science and solid-state physics. For example, Artificial Neural Network [20], Taguchi [21], and Genetic Algorithm [22]. Among these ways, the ANN is one of the strong computing systems for approaching different datasets to reach a solution [23]. This modeling technique is based on learning and subsequently the prediction of output responses [24]. ANN has been extensively employed in MA and due to the diverse major parameters in the milling process, it can estimate the desired outputs [25-27].

In this work, the process of transformation of the ordered phase into the amorphous and nanostructured phase during high-energy ball-milling was investigated by applying numerous analyses and state-of-the-art methods (Rietveld/MAUD). Therefore, the quantity of the produced AC at different times of ball-milling was estimated via analyzing the results of XRD patterns. In order to increase the produced AC, the MA was optimized by using two types of balls and increasing the milling time. Moreover, an artificial neural network was designed to predict the ultimate size of carbon crystallite during graphite milling by applying the effective variables.

Experimental

Materials

The high-purity flake of graphite (15 μm) was chosen as the precursor. The milling process was induced in a planetary ball mill with 10 gr of the graphite and 5 steel balls of 15 mm diameter and 32 steel balls of 10 mm diameter in the argon atmosphere. The ball-to-powder weight ratio was kept at 20:1 and the vial speed was 300 rpm and mechanical activation was performed at different times of ball-milling. Finally, the obtained amorphous carbon from the ball-milling process was subjected to heat treatment at 1400 ˚C for 3 h.

Characterization

The structural change in obtained samples was assessed using X-ray diffractometer (Philips X'Pert, Cu-Kα, λ=0/1542 nm). Atomic force microscope (Autoprobe Cp, contact mode, 1 Hz rate of scan), transmission electron microscopy (LEO912-AB operated at 100 kV), and field emission scanning electron microscopy (Mira 3-XMU) were used to study the structure of the activated carbon.

Results and Discussion

The X-ray diffraction patterns of graphite powder for various activation times are shown in Figure. 1. Unmilled graphite has a sharp peak at 26˚-27˚ and a broad peak at 43˚-46˚. These peaks become broader and shorter by increasing the milling time because of the enhancement of the surface area of particles, the development of

dislocations, and the creation of sub-grain boundaries.

The amorphization mechanism is not completely clear. It seems when crystallite size reaches a critical value, the conversion of the crystalline to amorphous phase occurs. Thermodynamically, a continuous decrease in the crystallite size, growing crystallite defects, and the lattice expansion rise the Gibbs free energy of the system to a higher level than the amorphous phase, and as a result, an amorphous structure will be formed [28]. If the grain size of carbon was reduced to the ultimate value of about 3 nm [14], the crystal structure of graphite changed to the amorphous structure due to the fracturing basal planes and destruction of graphite crystalline structure [29].

As seen in Figure. 1, the percentage of the amorphous phase, crystallite size, micro-strains, the average distance between the graphene planes (d002) were calculated using Rietveld/MAUD (Table 1). The crystallite size of carbon was decreased by increasing the milling time. Conversely, d002, the micro-strain, and the amount of amorphous phase were increased. 97% of the ordered carbon phase converted to the amorphous phase after 330 h of ball-milling. Similar to the changes of the XRD pattern, the crystallite size is decreased by increasing the activation time and finally is transferred to a completely disordered and metastable phase. It seems amorphization of carbon is similar to amorphization of ordered alloys according to the following sequence [28, 30]:

Ordered phase ➡ disordered phase ➡ nanocrystalline phase ➡ amorphous phase

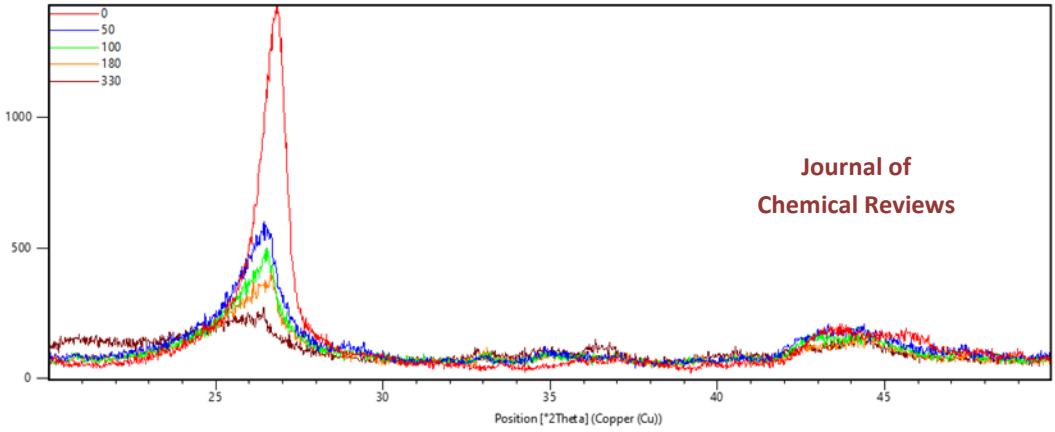

Figure 1. XRD pattern of ball-milled graphite at different time of milling.

Table 1. Characteristics of the crystal structure of graphite during the ball-milling process.

Time of Milling (h)	Percentage of Amorphous phase	Size of Crystallite (Å)	Strain	d_{002} (Å)
0	0	39	0.00613	**0.0332**
50	22	9.6	0.0175	**0.0337**
100	69	5.8	0.0219	**0.0337**
180	72	5.09	0.0223	**0.03376**
330	93	0.13	0.02507	**0.0339**

Previous studies [33-37,41] have reported various times for the production of amorphous carbon due to differences in the type of ball mill, ball to powder weight ratio, the milling speed, and other important items. In this research, the normal milling condition was used to prevent the fabrication of crumpled graphite layers which are produced during the MA. After 180 h of milling, no significant changes are observed in the X-ray diffraction pattern. There is some evidence to suggest that after a long time of milling of graphite (170-1000 h), there was no

change in the XRD pattern and crystallite size [19,31]. This is the result of a balance between dislocation motion and recovery and recrystallization processes, which cross slips do not lead to the reduction of grain size.

AFM image of the milled graphite after the annealing step is demonstrated in Figure 2 After the heat treatment, the morphology of the milled graphite converted to the plates of graphene and due to recrystallization, carbon particles are re-connected to each other. Indeed, the stress-relieving and reduction of crystalline defects led to minor changes in dimensions and the structure of AC. Consequently, the crystalline structure of nanostructured plates of graphene is formed. However, it seems that recrystallization does not occur in all powders.

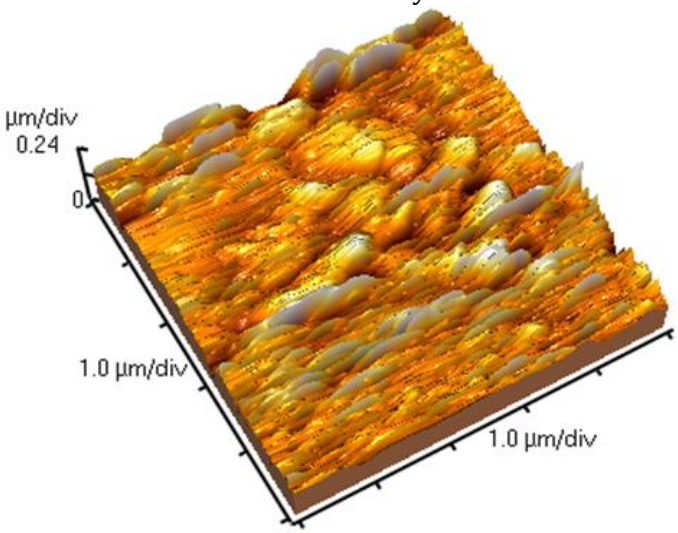

Figure 2. AFM image of ball-milled graphite after annealing at 1400 ˚C.

Figure 3 depicts the TEM and FE-SEM images of 330 h of ball-milled graphite after the heat treatment. A high percentage of graphite particles have a smaller size than 100 nm after the annealing step which reveals the suitable performance of the annealing stage. Owing to the high thermal stability of nanostructured graphite, the annealing of milled graphite did not lead to significant changes in the size of the graphite. Therefore, the non-stress nanostructured carbon with appropriate dimensional changes of particles is prepared by annealing of the milled graphite. It is also worth noting that there are a lot of particles smaller than 50 nm as seen from the arrows of the TEM figure.

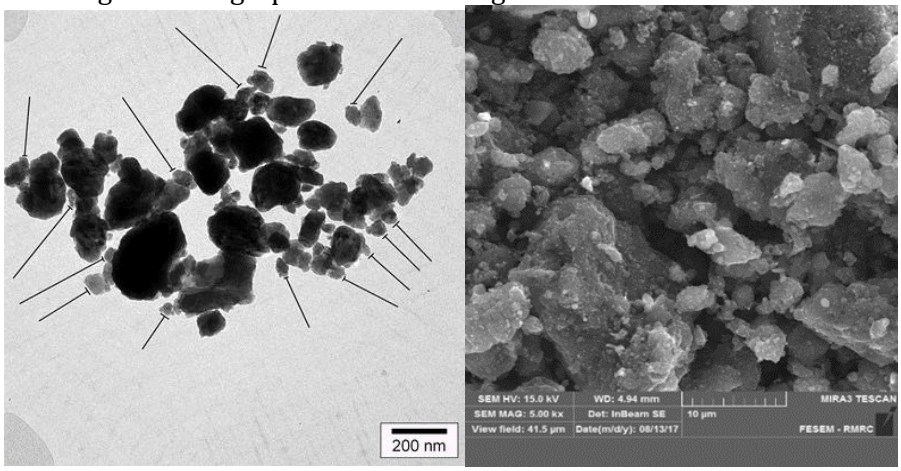

Figure 3. TEM and SEM images of the ball-milled graphite after heat treatment at 1400˚ C. Arrows show particles smaller than 50 nm.

Modeling Procedure

Artificial neural network theory is the parallel network model base on the biological learning process. This network including interconnected units known as neurons or nods. Neurons are the smallest computing elements and they are interconnected together by signals. These signals are transmitted several times from input to output and aggregate into layers [32]. The artificial network consists of three main layers including input, output, and hidden layers. The neural network learns by the training process including changing weights, adjusting the neuron's bias, and normalization of the output by activation functions. This cycle continues until the model approaches the requested output and achieves an acceptable error [20].

The relation of nods can be expressed by Equation 1:

$$x = f(\sum_{i=1}^{p} w_i x + b) \quad (1)$$

Where f is the activation function, the output x is created by the node in the layer, p is the number of factors in the layer, $w_i x$ is the weight, and b is the bias of the current neuron.

Collecting Experimental Data

Some of the most important factors in the MA which have an important effect on the final products are selected as the effective factors. These variables including milling time, milling speed, and ball-to-powder weight ratio. To predict the size of the crystallite size during ball-milling of graphite, required data was extracted from the valid international papers [15, 17-18, 33-37] and was collected in table 2.

Table. 2. Data sets of ball-milled graphite which is collected from previous works [15, 17-18, 33-37].

No.	BPR*	Vial speed (rpm)	Milling time (h)	Initial size of the crystallite (nm)	Final size of the crystallite (nm)	References
1	55	200	1	54.3	13.3	[17]
2	55	200	2	54.3	6.4	[17]
3	55	200	3	54.3	3.3	[17]
4	55	200	4	54.3	2.7	[17]
5	55	200	5	54.3	2.4	[17]
6	10	300	0.5	21	15.5	[15]
7	10	300	1	21	8.5	[15]
8	10	300	2	21	6	[15]
9	10	300	4	21	3.2	[15]
10	10	300	8	21	2.3	[15]
11	40	450	60	15.8	10.1	[33]
12	40	450	80	15.8	9.3	[33]
13	40	450	100	15.8	8.7	[33]
14	40	450	60	15.4	12.3	[33]
15	40	450	80	15.4	12.9	[33]
16	40	450	100	15.4	11.3	[33]
17	20	300	3	100	42.5	[34]
18	20	300	5	100	33	[34]
19	20	300	10	100	21	[34]
20	23	420	36	30	3.3	[18]
21	10	400	150	35	13	[35]
22	20	700	5	31.1	30.1	[36]
23	20	700	10	31.1	29.8	[36]
24	20	700	30	31.1	27.4	[36]
25	20	700	50	31.1	25.4	[36]

No.	BPR*	Vial speed (rpm)	Milling time (h)	Initial size of the crystallite (nm)	Final size of the crystallite (nm)	References
26	20	700	60	31.1	24.6	[36]
27	20	700	80	31.1	22.1	[36]
28	20	700	90	31.1	20.1	[36]
29	20	700	100	31.1	18.5	[36]
30	20	700	120	31.1	13.9	[36]
31	20	700	130	31.1	11.2	[36]
32	20	700	140	31.1	8.5	[36]
33	20	700	150	31.1	5.2	[36]
34	20	700	160	31.1	4.9	[36]
35	20	700	170	31.1	4.8	[36]
36	20	700	180	31.1	4.7	[36]
37	40	720	4	12	3.5	[37]
38	40	720	8	12	2.3	[37]
39	40	720	16	12	1.2	[37]
40	40	720	40	12	1.1	[37]

*BPR: Ball to Powder Ratio

The atmosphere of the ball-milling of graphite has a different effect on the destruction rate of the crystalline structure [38]. For example, this rate in argon is faster than air and oxygen since saturated carbon-oxygen bonds decrease the velocity of the destruction process [38, 15,39]. Moreover, mechanical milling of graphite in a wet environment has a lower effect on the crystalline structure of graphite and produces a higher number of contaminations than dry methods [40,41]. Therefore, the dry method and argon were chosen as the reaction atmosphere for the experimental process. Similarly, the collected data were selected only from the mention condition for more accuracy. To obtain the crystallite size, the Williamson-Hall law relation was used, according to Equation 2 [42]:

$$\beta cos\theta = 2\,\varepsilon sin\theta + 0.9(\frac{\lambda}{D}) \quad (2)$$

Where D is the crystallite size, β is the full width at half maximum (FWHM), θ is the brag angle, λ is the wavelength, and ε is the microstrain.

Model setup

ANN Architecture

29 and 11 data sets were chosen randomly for training and verification of the model, respectively. Feed-forward back propagation (BP) was used for the learning module. BP network has a high ability to achieve desired outputs and has been widely used in the ball-milling process to predict effective factors in similar studies [43-45].

In the BP algorithm, there are two stages in each round. First, the determination of a random value for all weight parameters (feed-forward). Then, changing the weights to achieve an output with less error and closer to the values (back-propagation). This process is repeated until the output of the network for all of the training data reaches the closest actual value [46].

The trial-and-error method was performed to specify the number of neurons in the hidden layers during the training process.

The designed network including one input and output layer, and two hidden layers containing 16 and 10 nodes in the first and second layers. The input factors are the initial size of the graphite crystallite, milling speed, ball to powder weight ratio, time of milling, and the final size of the crystallite considered as the output. The schematic diagram of the ANN is shown in Figure 4.

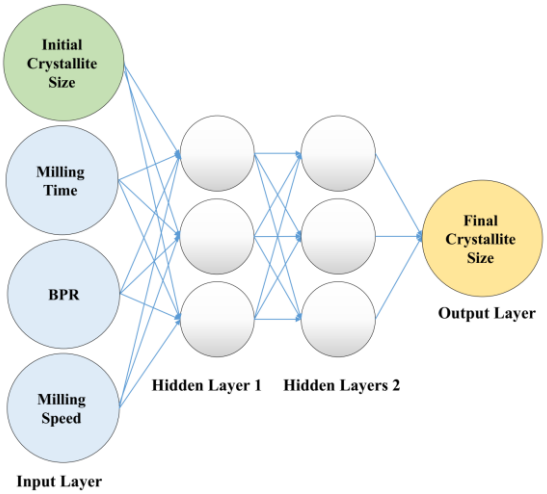

Figure 4. Architecture of the designed ANN.

The trained network and the finite element method were used for the calculation of the regression. MATLAB version R2014a due to its user-friendly interface and the Levenberg–Marquardt algorithm owing to fast learning capability [47], were used to write and train the network, respectively.

In addition, the log-sigmoid transfer function, which is S-shaped and non-linear, was employed as an activation function, according to Eq. 3 and Figure. 5:

$$f(x) = \frac{1}{1+e^{-x}} \quad (3)$$

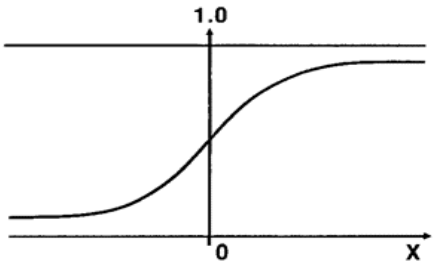

Figure 5. The log-sigmoid function curve

The log-sigmoid function has a high potential for learning the complex system and was used broadly in similar studies [27, 48].

All of the data sets have been homogenized and normalized (between 0.1 to 0.9) based on Eq. 4:

$$N = 0.8\left(\frac{x-x_{min}}{x_{max}-x_{min}}\right) + 0.1 \quad (4)$$

Where N is the normalized data, x_{min} and x_{max} are the minimum and maximum values of the variables, respectively.

Furthermore, the network's RMSE was computed by Eq. 5:

$$RMSE = \frac{1}{N}\sum_{1}^{N}\left(\frac{|\text{Actul value}-\text{Predicted value}|}{\text{Actul value}} \times 100\right) \quad (5)$$

ANN Results

For the purpose of test the accuracy of the trained model, regression analysis was applied. Certainly, the closer the regression value to 1 shows the better performance of the network. Figure. 6 provides information about the result of the regression analysis which the total regression is 0.99576. A comparison between actual and predicted values was conducted for verification of the created network. According to equation 5, the network's error was measured by 4%.

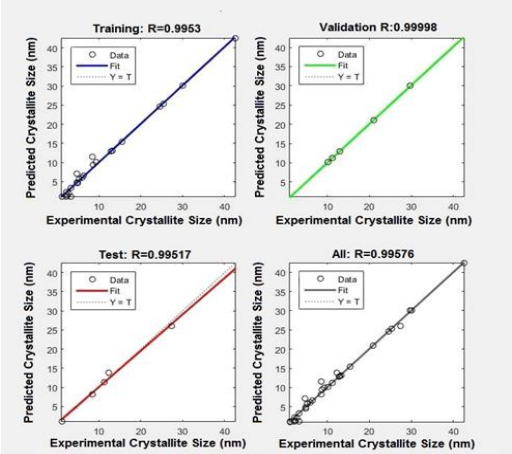

Figure 6. Regression analysis of the ANN model for prediction of carbon crystallite size.

Model verification

Figure 7 shows the experimental and predicted values for the crystallite size of carbon. It is completely noticeable that the created network with high precision predicts the actual values of the crystallite size. Consequently, it can be anticipated that the modeled network can predict other similar experiments with such a high approximation and dependability. Furthermore, the present network leads to better risk assessment of lab-based work regarding a lot of parameters in MA and the difficulty of setting them up.

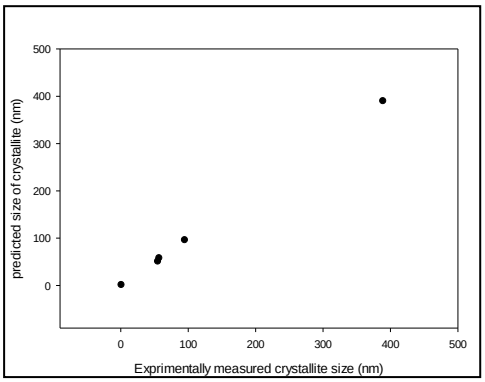

Figure 7. Comparison between experimental outcomes and predicted measurements.

Conclusion

In this research study, by optimizing the effective parameters in the ball-milling of graphite, a high percentage of the crystalline phase of carbon in the graphite was converted to a nanostructured, and eventually, the amorphous phase. The results of the quantitative phase analysis (Rietveld/MAUD) based on the obtained XRD patterns depicted that after 250 and 330 h of milling, near 91% and 93% of the graphite structure is changed to amorphous carbon, respectively. Furthermore, a feed-forward artificial neural network with 2 hidden layers consist of 16 and 10 neurons was used to predict the final crystallite size of carbon. The low RMSE and results of verification revealed that the designed network with high accuracy can predict the crystallite size of carbon during the mechanical activation of graphite.

Acknowledgments

This research is funded by the Shahid Bahonar University of Kerman and the authors declares that they have no conflict of interest. This work has not been published elsewhere and not submitted simultaneously for publication elsewhere.

Orcid

Seyed Oveis Mirabootalebi: https://orcid.org/0000-0001-5793-6238

Reza Mirahmadi Babaheydari: https://orcid.org/0000-0003-4724-374X

References

[1] A. Savvatimskiy. *Carbon at high temperatures,* **2015**, 134, 1-235. **[crossref], [Google Scholar], [Publisher]**

[2] S.O. Mirabootalebi, G.H. Akbari, R.M. Babaheydari, *Asian Journal of Nanosciences and Materials,* **2021**, 4, (In press). **[crossref], [Google Scholar], [Publisher]**

[3] F. Risplendi, G. Cicero, J.C. Grossman, *ACS Energy Letters*, **2017**, *2*, 882-888. **[crossref], [Google Scholar], [Publisher]**

[4] X. Zhang, X. Zhang, Z. Ren, J. Hu, M. Gao, H. Pan, and Y. Liu. *Frontiers in Chemistry*, **2020**, *8*. **[crossref], [Google Scholar], [Publisher]**

[5] S. Kundoo, S. Kar, *International Journal of Engineering, Science and Mathematics*, **2018**, *7*, 400-407. **[crossref], [Google Scholar], [Publisher]**

[6] S.O. Mirabootalebi, G. Akbari, *Int. J. Bio-Inorg. Hybr. Nanomater*, **2017**, *6*, 49-57. **[crossref], [Google Scholar], [Publisher]**

[7] S.O. Mirabootalebi, *Advanced Composites and Hybrid Materials*, **2020**, *3*, 336-343. **[crossref], [Google Scholar], [Publisher]**

[8] C.T. Toh, H. Zhang, J. Lin, A.S. Mayorov, Y.P. Wang, C.M. Orofeo, D.B. Ferry, H. Andersen, N. Kakenov, and Z. Guo. *Nature*, **2020**, *577*, 199-203. **[crossref], [Google Scholar], [Publisher]**

[9] Y.M. Manawi, A. Samara, T. Al-Ansari, M.A. Atieh. *Materials*, **2018**, *11*, 822. **[crossref], [Google Scholar], [Publisher]**

[10] D. Amans, M. Diouf, J. Lam, G. Ledoux, C. Dujardin. *Journal of colloid and interface science*, **2017**, *489*, 114-125. **[crossref], [Google Scholar], [Publisher]**

[11] D. Zhang, F. Liang, K. Ye, T. Qu, Y. Dai, *The Minerals, Metals & Materials Series,* **2020,** 735-741. **[crossref], [Google Scholar], [Publisher]**

[12] I.Y. Bu, L.Y. Kao, *International Journal of Nanomanufacturing*, **2017**, *13*, 161-169. **[crossref], [Google Scholar], [Publisher]**

[13] J.Tu, J. Wang, S. Li, W.L. Song, M. Wang, H. Zhu, S. Jiao, *Nanoscale*, 2019, 12537-12546. **[crossref], [Google Scholar], [Publisher]**

[14] Ö. Güler, E. Evin, *Fullerenes, Nanotubes and Carbon Nanostructures*, **2015**, *23*, 463-470. **[crossref], [Google Scholar], [Publisher]**

[15] J.C. Rietsch, R. Gadiou, C. Vix-Guterl, J. Dentzer, *Journal of alloys and compounds*, **2010**, *491*, L15-L19. **[crossref], [Google Scholar], [Publisher]**

[16] Q. Tang, J. Wu, H. Sun, S. Fang, *Journal of alloys and compounds*, **2009**, *475*, 429-433. **[crossref], [Google Scholar], [Publisher]**

[17] M. Francke, H. Hermann, R. Wenzel, G. Seifert, K. Wetzig, *Carbon*, **2005**, *43*, 1204-1212. **[crossref], [Google Scholar], [Publisher]**

[18] T. Fukunaga, K. Nagano, U. Mizutani, H. Wakayama, Y. Fukushima, *Journal of non-crystalline solids*, **1998**, *232*, 416-420. **[crossref], [Google Scholar], [Publisher]**

[19] N. Welham, J. Williams, *Carbon*, **1998**, *36*, 1309-1315. **[crossref], [Google Scholar], [Publisher]**

[20] S. Walczak, *Artificial neural networks*, **2019**, 40-53. **[crossref], [Google Scholar], [Publisher]**

[21] P.D. Berger, R.E. Maurer, G.B. Celli, in *Experimental Design.* **2018**, 449-480. **[crossref], [Google Scholar], [Publisher]**

[22] O. Kramer, *Genetic algorithm essentials*, **2017**, *679*, 11-19. **[crossref], [Google Scholar], [Publisher]**

[23] M. Van Gerven, S. Bohte, *Frontiers in Computational Neuroscience*, **2017**, *11*, 114. **[crossref], [Google Scholar], [Publisher]**

[24] A.M. Rashidi, A.R. Eivani, A. Amadeh, *Computational Materials Science*, **2009**, 45, 499-504. **[crossref], [Google Scholar], [Publisher]**

[25] V. Singh, P. Banerjee, S. Tripathy, V. Saxena, and R. Venugopal, *Journal of Powder Metallurgy and Mining*, **2013**, 2, 2-5. **[crossref], [Google Scholar], [Publisher]**

[26] S.O. Mirabootalebi, R.M. Babaheydari, *Iranian Journal of Organic Chemistry*, **2019**, *11*, 2731-2737. **[crossref], [Google Scholar], [Publisher]**

[27] R.M Babaheydari, S.O Mirabootalebi, *Journal of Environmental Friendly Materials*,

2020, *4*, 31-35. **[crossref], [Google Scholar], [Publisher]**

[28] C. Suryanarayana, Mechanical alloying and milling. *Progress in materials science*, **2001**, *46*, 1-184. **[crossref], [Google Scholar], [Publisher]**

[29] H. Hermann, T. Schubert, W. Gruner, N. Mattern, *Nanostructured materials*, **1997**, *8*, 215-229. **[crossref], [Google Scholar], [Publisher]**

[30] J.S.C. Jang, C.C. Koch, *Journal of Materials Research*, **1990**, *5*, 498-510. **[crossref], [Google Scholar], [Publisher]**

[31] S.A. Manafi, M.H. Amin, M.R. Rahimipour, E. Salahi, A. Kazemzadeh, *New Carbon Materials*, **2009**, *24*, 39-44. **[crossref], [Google Scholar], [Publisher]**

[32] I.N. Da Silva, D.H. Spatti, R.A. Flauzino, L.H.B. Liboni, S.F. dos Reis Alves, *Artificial neural networks,* **2017**, 21-28. **[crossref], [Google Scholar], [Publisher]**

[33] X. Yue, L. Li, R. Zhang, F. Zhang, *Materials characterization*, **2009**, *60*, 1541-1544. **[crossref], [Google Scholar], [Publisher]**

[34] M.P. Pileni, *New Journal of Chemistry*, **1998**, *22*, 693-702. **[crossref], [Google Scholar], [Publisher]**

[35] M.R. Johan, L.S. Moh, *Carbon*, **2013**, *8*, 1047-1056. **[crossref], [Google Scholar], [Publisher]**

[36] S. Manafi, M.R. Rahimipour, I. Mobasherpour, A. Soltanmoradi , *Journal of Nanomaterials*, **2012**, 2012. 1-8. **[crossref], [Google Scholar], [Publisher]**

[37] T.D. Shen, W.Q. Ge, K.Y. Wang, M.X. Quan, J.T. Wang, W.D. Wei, C.C. Koch, *Nanostructured materials*, **1996**, *7*, 393-399. **[crossref], [Google Scholar], [Publisher]**

[38] Y. Kuga, M. Shirahige, Y. Ohira, K. Ando. *Carbon*, **2002**, *40*, 695-701. **[crossref], [Google Scholar], [Publisher]**

[39] J.L. Li, L.J. Wang, G.Z. Bai, W. Jiang, *Scripta materialia*, **2006**, *54*, 93-97. **[crossref], [Google Scholar], [Publisher]**

[40] P. Kun, F. Wéber, C. Balázsi. *Open Chemistry*, **2011**, *9*, 47-51. **[crossref], [Google Scholar], [Publisher]**

[41] Ö. GÜLER, E. Evin, *Optoelectronics and Advanced Materials-Rapid Communications*, **2012**, *6*, 183-187. **[crossref], [Google Scholar], [Publisher]**

[42] G. Williamson, W. Hall, *Acta metallurgica*, **1953**, *1*, 22-31. **[crossref], [Google Scholar], [Publisher]**

[43] T. Varol, S. Ozsahin. *Particulate Science and Technology*, **2019**, *37*, 381-390. **[crossref], [Google Scholar], [Publisher]**

[44] T. Varol, A. Canakci, S. Ozsahin, *Journal of Alloys and Compounds*, **2018**, *739*, 1005-1014. **[crossref], [Google Scholar], [Publisher]**

[45] U. Devadiga, R.K.R. Poojary, P. Fernandes, *Journal of Materials Research and Technology*, **2019**, *8*, 3970-3977. **[crossref], [Google Scholar], [Publisher]**

[46] S. Panda, G. Panda, *Neural Processing Letters*, **2020**, 51, 1869-1889. **[crossref], [Google Scholar], [Publisher]**

[47] R. An, W.J. Li, H.G Han, J.F. Qiao, *35th Chinese Control Conference (CCC)*, **2016**, 3630-3635. **[crossref], [Google Scholar], [Publisher]**

[48] M. Zeraati, G.R. Khayati. *Journal of Ultrafine Grained and Nanostructured Materials*, **2018**, *51*, 183-192. **[crossref], [Google Scholar], [Publisher]**